An Experimental Study on Air-Water Two-Phase Flow Patterns in Pebble Beds

Bai Bofeng
Liu Maolong
Su Wang
Zhang Xiaojie

State Key Laboratory of Multiphase Flow in Power Engineering,
Xi'an Jiaotong University,
Xi'an 710049, China

An experimental study was conducted on the air-water two-phase flow patterns in the bed of rectangular cross sections containing spheres of regular distribution. Three kinds of glass spheres with different diameters (3 mm, 6 mm, and 8 mm) were used for the establishment of the test section. By means of visual observations of the two-phase flow through the test section, it was discovered that five different flow patterns occurred within the experimental parameter ranges, namely, bubbly flow, bubbly-slug flow, slug flow, slug-annular flow, and annular flow. A correlation for the bubble and slug diameter in the packed beds was proposed, which was an extended expression of the Tung/Dhir model, Jamialahmadi's model, and Schmidt's model. Three correlations were proposed to calculate the void friction of the flow pattern transition in bubble flow, slug flow, and annular flow based on the bubble model in the pore region. The experimental result showed that the modified Tung and Dhir model of the flow pattern transition was in better agreement with the experimental data compared with Tung and Dhir's model.
[DOI: 10.1115/1.4000337]

Keywords: two-phase flow, flow pattern, bubble, pebble bed

1 Introduction

Single and two-phase gas/liquid flow through the porous media composed of stationary granular particles occur frequently in fields of science and engineering, ranging from agriculture, biomedical science, mechanical engineering, nuclear engineering, chemical and petroleum engineering to food, and soil sciences [1]. In many of these applications, a liquid phase and a gaseous phase, mostly a vaporous phase, are involved [2]. If they are immiscible, each fluid has to be treated as a separate phase [3]. In all the instances it is necessary to predict the designing parameters such as friction factor, pressure drop, bubble size, void friction, flow pattern transition criteria, and heat and mass transfer coefficients for the determination of the desired operating conditions and the specifications [1]. Therefore, expressions are needed for the accurate prediction of these parameters in the porous media in which the fluids flow either as single phase or as gas/liquid mixtures.

Research efforts were made to recognize the flow patterns occurring when gas and liquid flow concurrently through the porous media [4,5]. The researchers observed different flow patterns, namely, the homogeneous, transitional, and heterogeneous regimes by establishing a constant liquid flow rate through the bed and then increasing the gas flow rate [5–7]. Chu et al. [8,9], based on their visual observations in the porous media composed of large-sized particles ($d_p \geq 6$ mm), reported a distinct change in the flow patterns with the increase in the void fraction. Tung and Dhir [7] modeled three stable flow patterns, namely, bubbly flow, slug flow, and annular flow and two transition flow patterns along the three stable flow patterns. And a model was proposed about the diameter of the bubble and the transition criteria for different flow patterns. A comparison of the model with the measured pressure gradient, as well as the void fractions of the isothermal air/water experiments by Chu et al. (Ref. [8]) revealed a good agreement with the experimental data, except that Chu et al. experimented on relatively larger particles (d_p=5.8, 9.9, and 19 mm). According to Tung and Dhir's study on the particles of d_p =5.8 mm, their model showed greater deviations for smaller particles [2]. Schmidt found that the assumption on gas bubbles in the pores became questionable for small particles and thus proposed some modifications to the original Tung/Dhir model for its application to particles of small diameters. The first modification concerned the diameter of the gas bubbles or the slugs and the second the flow pattern ranges used in the Tung/Dhir model [2].

In the present paper, the air-water two-phase flow patterns in the bed of rectangular cross sections containing spheres with different diameters (3 mm, 6 mm, and 8 mm) were measured with a high-speed video camera. The flow patterns were classified with their interface structure. A correlation for the bubble and slug diameter was proposed. A flow pattern map was also proposed on the basis of the modified Tung and Dhir model of the flow pattern transition.

2 Experimental Techniques

The present experiment aims to obtain the pertinent data on two-phase flow parameters for the coflow through the porous media. In the experiment, the porous layers are made up of glass particles and water and air are employed as the continuous and discontinuous phases, respectively. A brief description of the experiment is given in the following text.

2.1 Experimental Apparatus. A schematic diagram of the experimental apparatus for coflow experiments is shown in Fig. 1. The primary parts are a plexiglass test section, a water reservoir, a main centrifugal pump, and two valves for the control of the mass flow rate. Two Dwyer glass rotameters with different measure range are used to measure the gas flow with the uncertainty of ± 0.05 m^3/h and ± 0.03 m^3/h separately. The water flow is measured with an orifice mass flux meter with $\pm 0.5\%$ uncertainty, the inlet pressure of the test section is measured with a MPM498 static pressure transmitter with $\pm 0.1\%$ uncertainty, the pressure drop is measured with a Rosemount 3051 transmitter with $\pm 0.5\%$ uncertainty, and the bulk flow temperature is measured with a T-type thermocouple with $\pm 0.1\,^{\circ}C$ uncertainty. The gas-liquid flow in the pore scale of the particles is recorded by a high-speed video camera (Memrecam fx K3 2000 frames/s). A zone in the

Contributed by the Nuclear Division of ASME for publication in the JOURNAL OF ENGINEERING FOR GAS TURBINES AND POWER. Manuscript received July 17, 2009; final manuscript received August 7, 2009; published online January 27, 2010. Editor: Dilip R. Ballal.

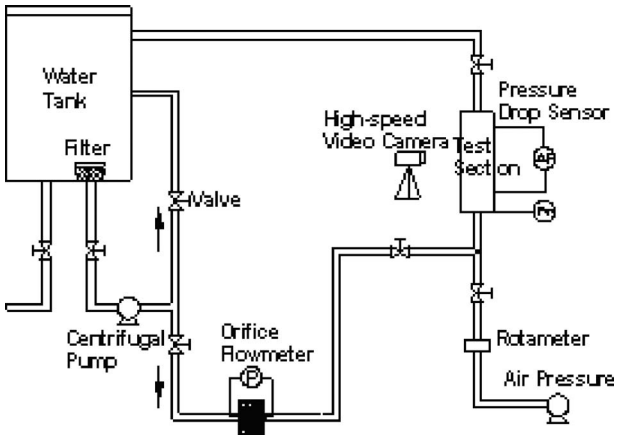

Fig. 1 Schematic diagram of the experimental apparatus for coflow studies

central part of the experimental bed with a width of 30 mm, and a height of 36 mm is focused. The images are transmitted for visualization to a 25 frames/s video movie. Three different types of packings composed of glass particles were employed, the specifications of which are shown in Table 1. And the ranges of Re number for the air-water flow in the each test section are shown in Table 2.

2.2 Experimental Procedures. Clean particles of a given size were filled into the test section with a certain height. After the formation of the bed, a predetermined flow rate of water was established through the porous layer. Thus, the packed bed was initially covered with water to ensure the complete wetting of the packings. When the liquid flow rate was kept constant at the desired one, gas was introduced into the bed. The gas flow rate was increased to the predetermined maximum one. On reaching the maximum gas flow rate, the gas flow rate was reduced to a low level. For both maximum and the reduced gas flow rate conditions, flow patterns were recorded with the high-speed video camera, and pressure drops and temperatures were measured for each set of gas and liquid flow rates.

3 Experimental Results

By means of visual observation of the two-phase flow through the test section, five different flow patterns are concluded within

Table 1 Specifications of the packing utilized

Case No.	1	2	3
Shape	Rectangle	Rectangle	Rectangle
Materials	Glass	Glass	Glass
Length (mm)	181.90	311.80	361.33
Width (mm)	311.80	57.00	78.00
Height (mm)	3.95	7.90	10.53
d_p (mm)	3.00	6.00	8.00
ε	0.341	0.378	0.398

Table 2 Ranges of Re number for the air-water flow in the each test section

d_p (mm)	Re	
	Min.	Max.
3.00	521	4194
6.00	573	9152
8.00	380	14713

Fig. 2 Bubbly flow in the pebble beds composed of 8 mm diameter particles

the experimental parameter ranges, namely bubbly flow, bubbly-slug flow, slug flow, slug-annular flow, and annular flow.

3.1 Bubbly Flow. Figure 2 shows the bubbly flow in the test section composed of the particles with a diameter of 8 mm. In the bubble regime, the liquid phase is continuous, and the gas phase is dispersed as small or large bubbles of different shapes. At high liquid and low gas flow rates, the gas phase is dispersed as small nearly spherical bubbles. When the gas flow rate increases, the bubbles become large and elongated [10]. In this regime, the tiny bubbles pass through the pore of the bed smoothly without significant collisions or coalescence, while the large bubbles pass through the pore more slowly with significant collisions or coalescence because they are strongly influenced by the structure of the pore. For particles diameter smaller than 6 mm, no pure bubbly flow was observed.

3.2 Bubbly-Slug Flow. Figure 3 shows the bubbly-slug flow in the test section composed of the particles with diameter of 8 mm and 6 mm, respectively. Bubbly-slug flow is the transitional flow from the bubbly flow to the slug flow. The transition is a smooth one, and there is a range of void fraction in which bubbles and slugs co-exist. As a result, the bubbly-slug flow is characterized by the co-existence of few discrete stable slugs and a vast number of bubbles in the continuous liquid phase. The slugs, characterized by the larger size, are formed by the significant collisions or coalescence of bubbles. In this flow pattern, the tiny bubbles pass through the pore of the bed easily without significant collisions or coalescence, while the large bubbles and slugs pass through the pore more slowly with significant collisions or coalescence because they are strongly influenced by the structure of the pore. For particle diameter equal to 3 mm, no pure bubbly flow and bubbly-slug flow were observed.

3.3 Slug Flow. Slug flow is characterized by the co-existence of a vast number of discrete stable slugs and small numbers of bubbles in the continuous liquid phase, and the slugs are packed together more densely, as shown in Fig. 4. In this regime, the slugs undergo even more significant and rapid collisions or coalescence than the bubbly-slug flow and assume a variety of sizes and shapes, such as triangle, semicircular, or V-shape.

3.4 Slug-Annular Flow. Figure 5 shows the slug-annular flow in the test section composed the particles with diameters of 8 mm, 6 mm, and 3 mm, respectively. The transition to the annular flow is also a smooth one, and there is a range of void fractions in

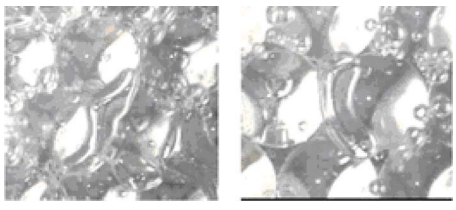

Fig. 3 Bubbly-slug flow in the pebble beds composed of 8 mm and 6 mm diameter particles

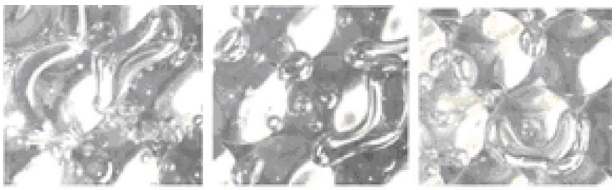

Fig. 4 Slug flow in the pebble beds composed of 8 mm, 6 mm, and 3 mm diameter particles

which the slug flow and the annular flow co-exist. As a result, the slug-annular flow, formed by the significant collisions or coalescence of slugs, is generally characterized by the co-existence of discrete stable slugs and a vast of continuous gas phase. In this regime, the slugs or small bubbles are merged by the continuous gas phase, which has a variety of shapes.

3.5 Annular Flow. Annular flow occurs at high gas superficial velocities and within the entire range of liquid superficial velocities. As shown in Fig. 6, in the annular flow, a liquid film is formed at the surface of the particles, while the continuous gas core flow cocurrently with the liquid phase. At very high gas flow rates some liquid is conceived to be detached from the liquid-gas interface and appears as entrained droplets.

Thus it is concluded that the bubble transformation mechanism is closely related to the pore structure, as well as the bubble size. The gravity exerts significant influences on the bubble transformation behavior [11]. During the experiments, it is discovered that a certain number of bubbles get trapped in the interstitials of the particles. These bubbles fail to move with the flow and constitute an inactive void fraction in the particulate bed. Holocher et al. [12] presented a kinetic model for dissolved gas transport in a porous medium, including interphase mass transfer with entrapped air bubbles.

4 Theoretical Model and Discussion

4.1 Void Fraction. A correlation for the slip ratio, S, can be represented as [13]

$$S = 1 + B_1\left(\frac{y}{1 + yB_2} - yB_2\right)^{0.5} \tag{1}$$

$$y = (1 - \beta)/\beta \tag{2}$$

Fig. 5 Slug-annular flow in the pebble beds composed of 8 mm, 6 mm, and 3 mm diameter particles

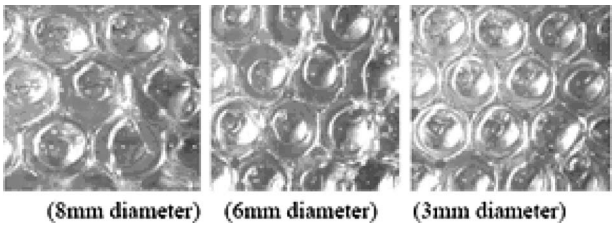

Fig. 6 Annular flow in the pebble beds composed of 8 mm, 6 mm, and 3 mm diameter particles

$$\beta = j_g\alpha/[j_g\alpha + j_l(1 - \alpha)] \tag{3}$$

$$B_1 = 1.578\ \mathrm{Re}_{l0}^{-0.19}(\rho_l/\rho_g)^{0.22} \tag{4}$$

$$B_2 = 0.0273\ \mathrm{We}_{l0}\ \mathrm{Re}_{l0}^{-0.51}(\rho_l/\rho_g)^{-0.08} \tag{5}$$

From what is mentioned above, the void fraction can be determined by

$$\alpha = 1/[1 + ((1 - \beta)/\beta)S] \tag{6}$$

Bao et al. [14] compared the above correlation with their microchannel void fraction data and reported a relatively good agreement. This void fraction method mentioned above is employed in the present study for the calculation of air/water two-phase flow void fractions applicable to the experimental ranges. The result shows that it fits the present experiment well.

4.2 Bubble and Slug Size. At low gas velocities, a homogeneous flow pattern prevails, and the tiny bubbles pass through the bed without significant collisions or coalescence. Since they flow practically at the same velocity as the liquid phase, the additional turbulence due to the second phase is minor. In this regime, the bubble diameter is generally determined by the pore size, the surface tension, and the buoyancy [1]

$$D_b = 0.09\left[\frac{d_p \times \sigma}{g(\rho_l - \rho_g)}\right]^{1/3} \tag{7}$$

In view of the similar consideration, in the work of Tung and Dhir [7], the value of D_b is taken as

$$D_b = 1.35\left[\frac{\sigma}{g(\rho_l - \rho_g)}\right]^{1/2} \tag{8}$$

where the constants of proportionality in the above two equations (0.09 and 1.35) are determined from photographs taken during the experiment. The slug length, on the other hand, is dependent on a delicate balance between the inertia forces, which tends to break it up, and the surface tension force, which tends to hold it together. A detailed analysis of the slug length is beyond the present study. Therefore, the length of the slug will be taken as [1,7]

$$L_b/D_b \approx 6 - 10 \tag{9}$$

As is mentioned above, Tung/Dhir model shows greater deviations for smaller particles. Given the diameter of the gas bubbles used by Tung and Dhir, this discrepancy is acceptable. Putting the value of the density difference between air and liquid, as well as the surface tension, into Eq. (8) yields a bubble diameter of $D_b = 3.75$ mm. Thus, the applied bubble diameter becomes larger than the pore diameter D_{pore} for small particles, which is contrary to the geometric ideas of the model. Additionally, the assumption about the gas bubbles in the pores becomes questionable for small particles. This leads to some modifications of the original Tung/Dhir model for the application of smaller particle diameters [2]. Based on the assumption of a cubic distribution of spherical particles and the present experiment, and in order to establish a connection with the original Tung/Dhir model, a modified bubble diameter is defined for convenience by

$$D_b^m = \min\left\{1.35\left[\frac{\sigma}{g(\rho_l - \rho_g)}\right]^{1/2}, 0.09\left[\frac{d_p \times \sigma}{g(\rho_l - \rho_g)}\right]^{1/3}\right\} \tag{10}$$

Therefore, there exists a critical particle diameter d_c. For air-water two-phase flow at 30°C, $d_c = 9.22$ mm. When the particle diameter is larger than d_c, the bubble diameter can be assumed to be constant.

4.3 Bubbly Flow. When the bubbles move along the surface of the particles, the number of bubbles per unit volume of the porous layer is given by the references [7,14]

$$N = \alpha\varepsilon/V_b \tag{11}$$

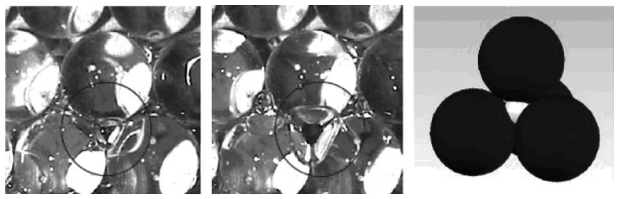

Fig. 7 Bubble model in the pore region

$$\alpha = NV_b/\varepsilon \tag{12}$$

At low void fractions the flow configuration is characterized by the motion of discrete bubbles. Although continuous breakup and reformation of the bubbles take place, the bubbles can be assumed to be superficial in shape with an average diameter D_b [7]. At a higher void fraction α_1 the bubbles merge to form slugs.

When d_p is larger than d_c, bubble diameter is nearly constant; as a result, both the volume of bubble V_b and the number of bubbles per unit volume of the porous layer are constant. So in terms of the Eq. (12), it is concluded that the void fraction α_1 is constant.

When d_p is smaller than d_c, as is shown in Fig. 7, the pore diameter, which is determined by the particle size, exerts significant influence on the bubble diameter which is determined by the Eq. (7). Thus the bubble volume is

$$V_b = \frac{\pi}{6}D_b^3 = 7.29 \times 10^{-4} \cdot \frac{\pi}{6}\frac{\sigma d_p}{g(\rho_l - \rho_g)} \tag{13}$$

As shown in the Fig. 7, when d_p is smaller than d_c, the pore region formed by four particles is filled out by the bubble, so the bubble diameter is nearly the same as the pore diameter. And the pore volume can be calculated by the Eq. (14)

$$V_{\text{pore}} \approx 0.026 \times d_p^3 \tag{14}$$

According to the bubble model shown in the Fig. 7, it can be assumed that the number of bubbles per unit volume of the porous layer is constant. Casting the Eq. (12) in terms of the bubble volume V_b with the Eq. (13), it is concluded that the void friction is proportional to the particle diameter d_p

$$\alpha_1 = 7.29 \times 10^{-4} \times \frac{\pi}{6}\frac{N}{\varepsilon g(\rho_l - \rho_g)}d_p \tag{15}$$

The average bubble size at the inlet of the porous can be assumed as constant, which can be calculated by the Eq. (8). The bubbles would be elongated when the pore size is smaller than the bubble size. Here we assume that the bubble diameter is equal to the equivalent pore diameter when the bubble is elongated. Thus, the volume of the bubble is

$$V_b = \pi/6D_b^3 = \pi D_{\text{pore}}^2 L_b/4 \tag{16}$$

For slug flow, its bubble length L_b is roughly equivalent to the particle diameter. Casting $L_b = D_b$ in terms of the Eq. (14) and Eq. (16), the particle diameter, d_p, is equal to 6.38 mm. As a result, for particles diameter smaller than 6.38 mm, no pure bubbly flow would be observed, which agrees with the present experimental result.

4.4 Slug Flow. As the void fraction increases the slugs are packed together more densely. However, there is an upper limit value α_3, beyond which the slugs will merge to form continuous gas paths. At this void fraction the transition to the annular flow occurs. In obtaining the void fraction corresponding to this transition it is conceptualized that the slugs are replaced by the spheres which fill up the pores. The number of slugs per unit volume of the porous layer is given by reference [7]

$$N = \frac{\alpha_3 \varepsilon}{V_s} \tag{17}$$

$$\alpha_3 = NV_s/\varepsilon \tag{18}$$

When d_p is greater than d_c, the slug diameter tends to remain constant; as a result, both the volume of slug V_s and the number of slugs per unit volume of the porous layer are constant. So in terms of Eq. (18), it is concluded that void fraction is constant. While d_p is smaller than d_c, the pore diameter, which is determined by the particle size, has significant influence on the slug diameter, which is determined by Eq. (7). The slug volume is calculated with Eq. (19).

$$V_s = \frac{\pi}{6}D_b^2 L_b \tag{19}$$

When d_p is smaller than d_c, the pore region is filled up by the slug, so the slug diameter is nearly the same as the pore diameter. Therefore, it can be assumed that the number of slugs per unit volume of the porous layer is constant. Casting the Eq. (18) in terms of the slug volume V_s, it is concluded that the void friction is proportional to the particle diameter d_p.

4.5 Bubbly-Slug Flow. Bubbly-slug flow is the transition from the bubbly flow to the slug flow. At void fraction α_1, some bubbles start to merge into slugs. The transition from the bubbly to the slug flow, however, is a smooth one and there is a range of void fraction in which bubbles and slugs co-exist. The upper bound of this region can be obtained by assuming that the transition is complete when the void fraction corresponds to the lightest packing of slugs [7]. As a result, the mentioned characteristics above of the bubbly flow and the slug flow are similar to those of the bubble-slug flow: when d_p is greater than d_c, the void fraction α_2 is constant; when d_p is smaller than d_c, the void friction is proportional to the particle diameter d_p.

4.6 Annular Flow. At the void fractions higher than α_4, the slugs merge thoroughly to form continuous gas flow paths. For this reason, it is assumed that the diameter of the continuous gas is nearly the same as the diameter of the slugs. The liquid then flows along the surface of the particles in the form of a thin film. At very high gas flow rates it is conceivable that some liquid is detached from the liquid-gas interface and appear as entrained droplets, which occurs at void fractions very close to unity. Therefore, in the present model, the annular flow is assumed to persist up to $\alpha \approx 1$ [7]. Based on the above assumption, the same conclusion is made that when d_p is greater than d_c, the void fraction α_4 is constant; when d_p is smaller than d_c, the void friction is proportional to the particle diameter d_p.

4.7 Slug-Annular Flow. Departure from the slug flow occurs at void fraction α_3. The transition to the annular flow is also a smooth one with an upper bound α_4. The void fraction is α_4 taken to be one corresponding to the densest possible packing of the pore space by the equivalent spheres. The densest packing occurs when the equivalent spheres are distributed in a rhombohedra array, i.e., slugs have to merge thoroughly if more gas is present in the pores [7]. As a result, the mentioned characteristics above of the slug flow are similar to those of the slug-annular flow: when d_p is greater than d_c, the void fraction α_3 is constant; when d_p is smaller than d_c, the void friction is proportional to the particle diameter d_p.

4.8 Flow Pattern Map. Based on the above discussion and the work of Tung, Dhir, and Schmidt, the modifications to the flow pattern given by Schmidt [2] are shown in Fig. 8 by the solid lines. As can be seen, the flow pattern is well predicted by the modified Tung/Dhir model [15].

5 Conclusion

A correlation for the bubble and the slug diameter in the pebble beds is proposed. This correlation is an extended expression of the Tung/Dhir model, Jamialahmadi's model [1] and Schmidt's model

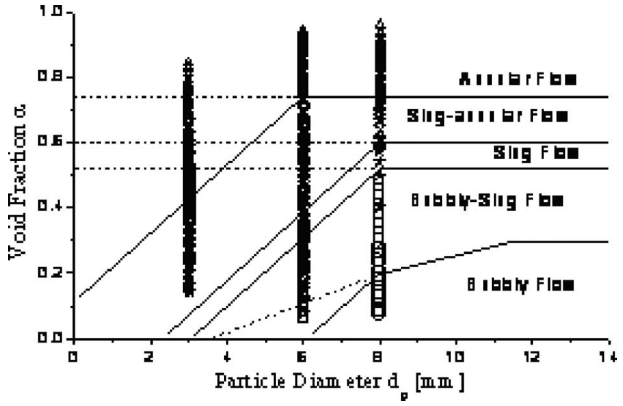

Fig. 8 Flow pattern map of the modified Tung/Dhir model

[2]. Three correlations are proposed for the calculation of the void friction of the flow pattern transition in bubble flow, slug flow, and annular flow based on the bubble model in the pore region. The experimental results show that the modified Tung/Dhir model agrees well with the present experiment. The void fraction method derived by Premoli et al. [13] is used for the calculation of air/water two-phase flow void fractions covering the entire experiment range. The result shows that this method fits the present experiment well.

Acknowledgment

This work was financially supported by the National Nature Science Foundation of China for Creative Research Groups under the Contract No. 50821064.

Nomenclature

d_c = critical particle diameter, m
d_e = equivalent particle diameter $[6V_p/S_p]$, m
d_p = particle nominal diameter, m
d_s = equivalent volume sphere diameter $[(6V_p/\pi)^{1/3}]$, m
D = diameter of column, m
D_b = bubble or slug diameter, m
D_{pore} = equivalent pore diameter $[(6V_{\text{pore}}/\pi)^{1/3}]$, m
j = superficial velocity, m/s
L = length of slug, m
Re_{l0} = Reynolds number when all fluid is liquid, $[\text{Re}_{l0}=GD/\mu_l]$
S = slip ration
V_b = volume of bubble, m^3
V_{pore} = volume of single pore, m^3
We_{l0} = Weber numbers when all fluid is liquid, $[\text{We}_{l0}=G^2D/(\sigma\rho_l)]$

Greek Letters

α = void fraction
β = volume void fraction
ε = porosity
$\bar{\varepsilon}$ = average bed porosity
σ = surface tension of water,
μ_α = dynamic viscosity of a-phase, Pa s
ρ_α = density of a-phase, kg/m^3

Subscripts

α = gas or liquid phase
b = bubble
g = gas phase
l = liquid phase
p = particle
s = slug

References

[1] Jamialahmadi, M., Müller-Steinhagen, H., and Izadpanah, M. R., 2005, "Pressure Drop, Gas Hold-Up and Heat Transfer During Single and Two-Phase Flow Through Porous Media," Int. J. Heat Fluid Flow, **26**(1), pp. 156–172.
[2] Schmidt, W., 2007, "Interfacial Drag of Two-Phase Flow in Porous Media," Int. J. Multiphase Flow, **33**(6), pp. 638–657.
[3] Tung, V. X., and Dhir, V. K., 1990, "Finite Element Solution of Multi-Dimensional Two-Phase Flow Through Porous Media With Arbitrary Heating Conditions," Int. J. Multiphase Flow, **16**(6), pp. 985–1002.
[4] Dukler, A. E., Fabre, J. A., McQuillen, J. B., and Vernon, R., 1987, "Gas Liquid Flow at Microgravity Conditions-Flow Patterns and Their Transitions," ASME Paper No. A88-42829 17-34.
[5] El Hajal, J., Thome, J. R., and Cavallini, A., 2003, "Condensation in Horizontal Tubes, Part 1: Two-Phase Flow Pattern Map," Int. J. Heat Mass Transfer, **46**(18), pp. 3349–3363.
[6] Dankworth, D., Kevrekidis, I., and Sundaresan, S., 1990, "Dynamics of Pulsing Flow in Trickle Beds," AIChE J., **36**(4), pp. 605–621.
[7] Tung, V. X., and Dhir, V. K., 1988, "A Hydrodynamic Model for Two-Phase Flow Through Porous Media," Int. J. Multiphase Flow, **14**(1), pp. 47–65.
[8] CHU, W., Dhir, V. K., and Marshall, J. S., 1983, "Study of Pressure Drop, Void Fraction and Relative Permeabilities of Two-Phase Flow Through Porous Media," AIChE Symp. Ser., **79**(225), pp. 224–235.
[9] Chu, W., Lee, H., Dhir, V. K., and Catton, I., 1984, "Hydrodynamics of Two Phase Flow Through Homogeneous and Stratified Porous Layers," School of Medicine, California University, Los Angeles, CA, Paper No. NUREG/CR-3615.
[10] Benkrid, K., Rode, S., Pons, M. N., Pitiot, P., and Midoux, N., 2002, "Bubble Flow Mechanisms in Trickle Beds—An Experimental Study Using Image Processing," Chem. Eng. Sci., **57**(16), pp. 3347–3358.
[11] Fang, C., Peng, X. F., and Yang, Z., 2004, "Visualization of Liquid-Vapor Two-Phase Flow in Porous Media," Sixth International Symposium on Heat Transfer, Beijing, China, pp. 424–429.
[12] Holocher, J., Peeters, F., Aeschbach-Hertig, W., Kinzelbach, W., and Kipfer, R., 2003, "Kinetic Model of Gas Bubble Dissolution in Groundwater and Its Implications for the Dissolved Gas Composition," Environ. Sci. Technol., **37**(7), pp. 1337–1343.
[13] Triplett, K. A., Ghiaasiaan, S. M., Abdel-Khalik, S. I., LeMouel, A., and McCord, B. N., 1999, "Gas-Liquid Two-Phase Flow in Microchannels Part II: Void Fraction and Pressure Drop," Int. J. Multiphase Flow, **25**(3), pp. 395–410.
[14] Bao, Z., Bosnich, M., and Haynes, B., 1994, "Estimation of Void Fraction and Pressure Drop for Two-Phase Flow in Fine Passages," Chem. Eng. Res. Des., **72a**, pp. 625–632.
[15] Alexiadis, A., 2007, "Bubble Dispersion Patterns in Bubbly-Flow Released From a Porous Plug Into a Gas-Stirred Ladle," Appl. Math. Model., **31**(8), pp. 1534–1547.